Natural convection in a horizontal fluid layer periodically heated from above and below

M. Z. Hossain* and J. M. Floryan

Department of Mechanical and Materials Engineering, The University of Western Ontario, London, Ontario, Canada N6A 5B9

(Received 23 March 2015; revised manuscript received 3 June 2015; published 13 August 2015)

Natural convection in a horizontal slot heated from above and from below has been considered. Each heating has a certain spatial distribution. It has been demonstrated that a wide variety of convection patterns can be generated by changing the relative position of both heating patterns. A significant intensification of convection, compared to convection resulting from heating applied at one wall only, results if there is no phase shift between both patterns, while a significant reduction of convection results from the phase shift corresponding to half of the heating wavelength. The system generates a nonzero mean shear stress at each wall for all phase shifts except shifts corresponding to half of and one full heating wavelength. This effect, which is generated within one convection cell, gives rise to a global force which may lead to a thermally induced drift of the walls if such a drift was allowed.

DOI: 10.1103/PhysRevE.92.023015 PACS number(s): 44.25.+f

I. INTRODUCTION

The natural convection in a horizontal slot is typically associated with spatially homogeneous heating applied at the lower surface and is referred to as the Rayleigh-Bénard (RB) convection [1,2]. It results from transition from a conductive state of equilibrium when the critical conditions are met [3–6]. The onset of the RB convection can be affected by inhomogeneities in the boundary temperatures resulting in various forms of symmetry breaking [7].

Inhomogeneous heating creates horizontal density variations which lead to motions frequently referred to as horizontal convection [8–11]. These gradients create different vertical pressure distributions at various horizontal locations which, in turn, create horizontal pressure gradients. The resulting configurations are statically unstable resulting in the fluid movement regardless of the intensity of the heating. Identical motions can be generated by the same heating applied either from below or from above if one accounts for the up-down symmetry [12]. The spatial pattern is locked in with the heating pattern but only for small convection intensity. Higher intensities result in secondary states which might have different patterns. There are an uncountable number of possible heating patterns but a systematic study and categorization of their effects are not yet available. A complete analysis of the simplest pattern consisting of sinusoidal heating with an arbitrary wavelength has been given only recently [13] and has led to the concept of structured convection. Such convection affects contaminant transport in urban environments as local heating rates are determined by the dissimilar thermal properties of roofs, streets, and parks. It affects rural environments where local circulation is driven by variations in the heating rates of forests, fields, and lakes. The insulating effect of continents on the mantle convection within the Earth represents a spatially structured convection with heating from above [14]. Similar problems are found in geological applications where a system of fractures, leads, and polynyas in sea ice leads to convection in both the ocean and atmosphere [15]. Spatial variability can also result from the use of mixed insulating and conducting boundary conditions; see [16] for a good review. The heat island effect [17] provides another example. One can further look at systems of localized fires and prediction of their propagation [18], systems of computer chips, thermal patterning in microfluidic devices and so on, where combinations of the upper and lower heating are likely to occur.

In the laminar case, one could assume that the observable structure of convection should be the same as the pattern of the imposed heating. This so-called primary convection may, however, undergo transition to secondary states resulting in the convection pattern different from the imposed heating. The onset conditions are dictated by the interplay between two instability mechanisms, the RB mechanism, and the spatial parametric resonance. A detailed description of the system response for the simplest sinusoidal heating demonstrates that the secondary state may have either the form of longitudinal rolls (rolls parallel to the primary rolls), or the form of transverse rolls (rolls orthogonal to the primary rolls), or the form of oblique rolls depending on the heating wave number [19]. It has been shown that the wave number locking between primary and secondary convection occurs under certain conditions and that noncommensurate flow structures are possible. The same structures are observed when the sinusoidal heating is applied to the upper wall [12]. It is also known that a combination of periodic heating and horizontal forced convection leads to a drag reduction through an effect similar to the superhydrophobic effect [20]; this is referred to as the superthermohydrophobic effect [21,22]. Combination of periodic and uniform heating amplifies this effect [23] but its usefulness is limited by the system instabilities, regardless of whether the heating is applied to the lower or to the upper wall [24].

The main objective of this analysis is to study the properties of natural convection driven by two heating patterns, one applied at the upper wall and one at the lower wall. We focus our attention on the simplest patterns characterized by a single wave number, two amplitudes, and a phase shift between them. A model problem and the relevant formulation are discussed in Sec. II. The solution method is described in Sec. III. Results are discussed in Sec. IV. Section V provides a short summary of the main conclusions.

*mhossa7@uwo.ca

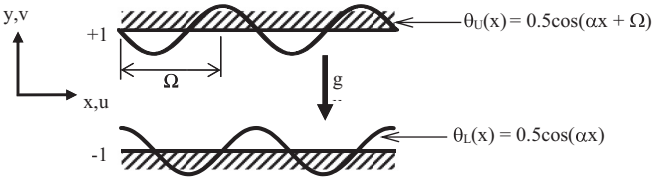

FIG. 1. Sketch of the system configuration.

II. PROBLEM FORMULATION

Consider fluid confined between two parallel walls extending to $\pm\infty$ in the x direction and placed at a distance 2h apart from each other with the gravitational acceleration g acting in the negative y direction, as shown in Fig. 1. The fluid is incompressible and Newtonian with thermal conductivity k, specific heat c, thermal diffusivity $\kappa = k/\rho c$, kinematic viscosity ν, dynamic viscosity μ, thermal expansion coefficient Γ and variations of the density ρ that follow the Boussinesq approximation. All material properties are evaluated at the mean wall temperature T_R which is used as the reference temperature. The lower and upper walls are subject to periodic heating with phase difference Ω between them, resulting in the walls' temperatures of the form

$$\theta_L(x) = \cos(\alpha x)/2, \tag{2.1}$$

$$\theta_U(x) = \cos(\alpha x + \Omega)/2, \tag{2.2}$$

where subscripts L and U refer to the lower and upper walls, respectively; θ_L denotes the relative temperature of the lower wall scaled with the amplitude of its peak-to-peak variations $T_{p,L}$, i.e., $\theta_L = (T - T_R)/T_{p,L}$; θ_U denotes the similarly defined relative temperature of the upper wall; T denotes the absolute temperature; $\lambda = 2\pi/\alpha$ is the wavelength of the heating; and the half channel height h has been used as the length scale. The horizontal temperature gradients lead to natural convection and the resulting temperature field can be represented as

$$\theta(x,y) = \mathrm{Ra}_{p,L}\,\theta_{0,L}(x,y) + \mathrm{Ra}_{p,U}\,\theta_{0,U}(x,y) + \theta_1(x,y), \tag{2.3}$$

where $\theta_{0,L}$ stands for the conductive temperature field associated with the lower wall heating, $\theta_{0,U}$ stands for the conductive temperature field associated with the upper wall heating, θ_1 denotes the temperature modifications associated with convection, and θ stands for the complete temperature field scaled with $\nu k/(g\Gamma h^3)$ as the temperature scale. $\mathrm{Ra}_{p,L} = g\Gamma h^3 T_{p,L}/(\nu k)$ and $\mathrm{Ra}_{p,U} = g\Gamma h^3 T_{p,U}/(\nu k)$ are the lower and upper periodic Rayleigh numbers expressing the intensity of the heating applied at these walls. The present temperature scaling is preferential for systems exposed to multiple heating sources as it permits independent variations of each source. Use of scaling based on the amplitude of one heating source is suitable for systems exposed to just one source [19]; it can be used with multiple sources but results have to be expressed in terms of ratios of amplitudes of these sources [23].

The solution for the conductive temperature field is of the form

$$\begin{aligned}\theta_{0,L}(x,y) &= \theta_{0,L}^{(1)}(y)\,e^{i\alpha x} + \theta_{0,L}^{(-1)}(y)\,e^{-i\alpha x},\\ \theta_{0,U}(x,y) &= \theta_{0,U}^{(1)}(y)\,e^{i\alpha x} + \theta_{0,U}^{(-1)}(y)\,e^{-i\alpha x},\end{aligned} \tag{2.4a}$$

where

$$\begin{aligned}\theta_{0,L}^{(1)}(y) &= [-\sinh(\alpha y)/\sinh(\alpha) + \cosh(\alpha y)/\cosh(\alpha)]/8,\\ \theta_{0,U}^{(1)}(y) &= e^{i\Omega}[\sinh(\alpha y)/\sinh(\alpha) + \cosh(\alpha y)/\cosh(\alpha)]/8.\end{aligned} \tag{2.4b}$$

$\theta_{0,L}^{(-1)} = \theta_{0,L}^{(1)*}$ and $\theta_{0,U}^{(-1)} = \theta_{0,U}^{(1)*}$ are the reality conditions, and stars denote the complex conjugate. The field equations for the stationary flow field and the temperature modifications have the form

$$u\frac{\partial u}{\partial x} + v\frac{\partial u}{\partial y} = -\frac{\partial p}{\partial x} + \nabla^2 u, \tag{2.5a}$$

$$\begin{aligned}u\frac{\partial v}{\partial x} + v\frac{\partial v}{\partial y} = &-\frac{\partial p}{\partial y} + \nabla^2 v + \mathrm{Pr}^{-1}\theta_1 + \mathrm{Ra}_{p,L}\mathrm{Pr}^{-1}\theta_{0,L}\\ &+\mathrm{Ra}_{p,U}\mathrm{Pr}^{-1}\theta_{0,U},\end{aligned} \tag{2.5b}$$

$$\begin{aligned}&u\left(\mathrm{Ra}_{p,L}\frac{\partial\theta_{0,L}}{\partial x} + \mathrm{Ra}_{p,U}\frac{\partial\theta_{0,U}}{\partial x} + \frac{\partial\theta_1}{\partial x}\right)\\ &+ v\left(\mathrm{Ra}_{p,L}\frac{\partial\theta_{0,L}}{\partial y} + \mathrm{Ra}_{p,U}\frac{\partial\theta_{0,U}}{\partial y} + \frac{\partial\theta_1}{\partial y}\right) = \mathrm{Pr}^{-1}\nabla^2\theta_1,\end{aligned} \tag{2.5c}$$

$$\frac{\partial u}{\partial x} + \frac{\partial v}{\partial y} = 0, \tag{2.5d}$$

where $(u,\ v)$ are the components of the velocity vector in the $(x,\ y)$ directions scaled with the convective velocity scale $U_v = \nu/h$, p denotes pressure scaled using ρU_v^2, ∇^2 denotes the Laplace operator, and $\mathrm{Pr} = \nu/k$ denotes the Prandtl number. The boundary conditions consist of the no-slip, the no-penetration, and the thermal boundary conditions of the form

$$u(\pm 1) = 0,\ \ v(\pm 1) = 0,\ \ \theta_1(\pm 1) = 0. \tag{2.6}$$

Problems (2.5) and (2.6) have been solved by expressing the velocity component using the stream function defined in the usual manner, i.e., $u = \partial\psi/\partial y$, $v = -\partial\psi/\partial x$, eliminating pressure and using spectrally accurate discretization based on the Fourier expansions in the horizontal direction and the Chebyshev expansions in the vertical direction. Details can be found in Ref. [25] together with testing of numerical accuracy. The reader may note that introduction of the stream function does not imply existence of the net mean flow in the horizontal direction [22,23].

The postprocessing involves evaluation of the wall shear stresses acting on the fluid at the upper (τ_U) and lower (τ_L) walls, i.e.,

$$\tau_U = \left.\frac{\partial u}{\partial y}\right|_{y=1}, \quad \tau_L = -\left.\frac{\partial u}{\partial y}\right|_{y=-1}. \tag{2.7}$$

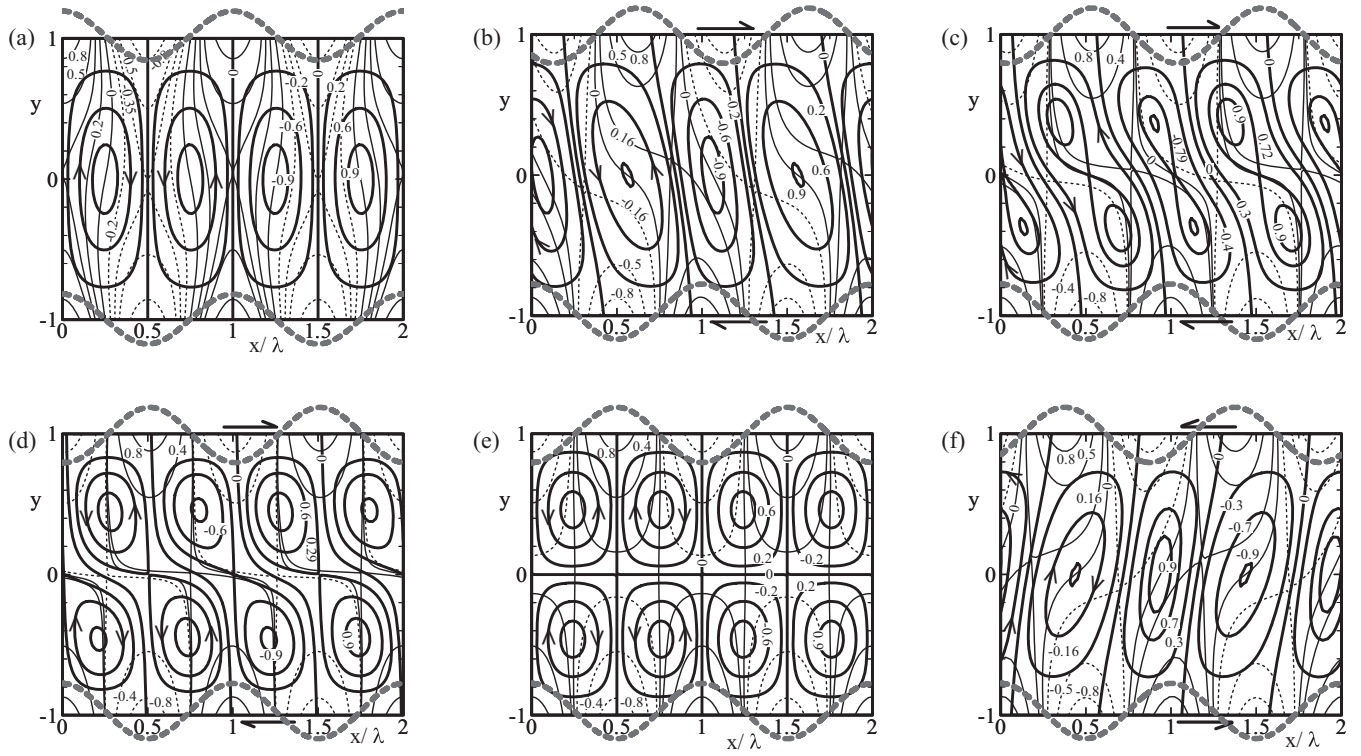

FIG. 2. Flow and temperature patterns for $\mathrm{Ra}_{p,L} = \mathrm{Ra}_{p,U} = 200$, $\mathrm{Pr} = 0.71$, $\alpha = 1.6$ and $\Omega = 0$, $3\pi/4$, $3.7\pi/4$, $3.9\pi/4$, π, $5\pi/4$ are displayed in (a)–(f), respectively. The thick solid lines correspond to the streamlines, and the thin solid and dashed lines correspond to the positive and negative isotherms, respectively. Arrows show direction of the mean stress acting on the fluid. Gray dashed lines illustrate temperature of the wall.

Their average values can be expressed as

$$\tau_{av,L} = \frac{1}{\lambda}\int_0^{\lambda}\left(-\left.\frac{\partial u}{\partial y}\right|_{y=-1}\right)dx, \tag{2.8a}$$

$$\tau_{av,\mathrm{U}} = \frac{1}{\lambda}\int_0^{\lambda}\left(\left.\frac{\partial u}{\partial y}\right|_{y=1}\right)dx. \tag{2.8b}$$

The reader may note that the flow remains stationary even for nonzero $\tau_{av,L}$ and $\tau_{av,U}$ as it is assumed that the walls are not allowed to move. The heat fluxes leaving the walls are expressed in terms of the Nusselt numbers Nu_L and Nu_U for the lower and upper walls, respectively, defined as

$$\mathrm{Nu}_U = \mathrm{Ra}_{p,L}\left.\frac{\partial\theta_{0,L}}{\partial y}\right|_{y=1} + \mathrm{Ra}_{p,U}\left.\frac{\partial\theta_{0,U}}{\partial y}\right|_{y=1} + \left.\frac{\partial\theta_1}{\partial y}\right|_{y=1}, \tag{2.9a}$$

$$\mathrm{Nu}_L = -\mathrm{Ra}_{p,L}\left.\frac{\partial\theta_{0,L}}{\partial y}\right|_{y=-1} - \mathrm{Ra}_{p,L}\left.\frac{\partial\theta_{0,U}}{\partial y}\right|_{y=-1} - \left.\frac{\partial\theta_1}{\partial y}\right|_{y=-1}. \tag{2.9b}$$

The net heat flux between the walls is expressed in term of the average Nusselt number of the form

$$\mathrm{Nu}_{av} = \mathrm{Nu}_{av,L} = \mathrm{Nu}_{av,U} = \frac{1}{\lambda}\int_0^{\lambda}\left(-\left.\frac{\partial\theta}{\partial y}\right|_{y=-1}\right)dx. \tag{2.10}$$

The horizontal heat fluxes along each wall can be measured in terms of the periodic part of the heat flux leaving the heated segment of each wall. This heat flux can be expressed in terms of the horizontal Nusselt numbers defined as

$$\begin{aligned}\mathrm{Nu}_{h,U} &= \frac{2}{\lambda}\int_{-\lambda/4-\Omega/\alpha}^{\lambda/4-\Omega/\alpha}\left.\frac{\partial\theta}{\partial y}\right|_{y=1}dx - \frac{1}{2}\mathrm{Nu}_{av,U},\\ \mathrm{Nu}_{h,L} &= -\frac{2}{\lambda}\int_{-\lambda/4}^{\lambda/4}\left.\frac{\partial\theta}{\partial y}\right|_{y=-1}dx + \frac{1}{2}\mathrm{Nu}_{av,L}.\end{aligned} \tag{2.11}$$

III. DISCUSSION OF RESULTS

Most of the presented results have been obtained for $\mathrm{Pr} = 0.71$ as it closely approximates properties of air. Flow and isotherm patterns for different phase shifts between the upper and lower heating patterns are displayed in Fig. 2. Convection consists of counter-rotating rolls of equal strength when the hot spots are above each other [$\Omega = 0$; see Fig. 2(a)] with columns of heated fluid centered around the hot spots and moving upwards and columns of cooled fluid centered around the cold spots and moving downwards. Fluid elements rotate inside cells and periodically come closer to the upper or lower walls, facilitating the net heat transfer between the walls. Use of the phase difference of $\Omega = 3\pi/4$ results in rolls of unequal strength tilted in the negative x direction [Fig. 2(b)]. The upward moving heated fluid concentrates in the tilted columns connecting the upper and lower hot spots, and the cooled fluid moving downwards concentrates in tilted columns connecting the cold spots. Further increase of the phase shift leads to an increase of the tilting and, eventually, to a division of rolls into two layers. The start of this process is illustrated in Fig. 2(c) for

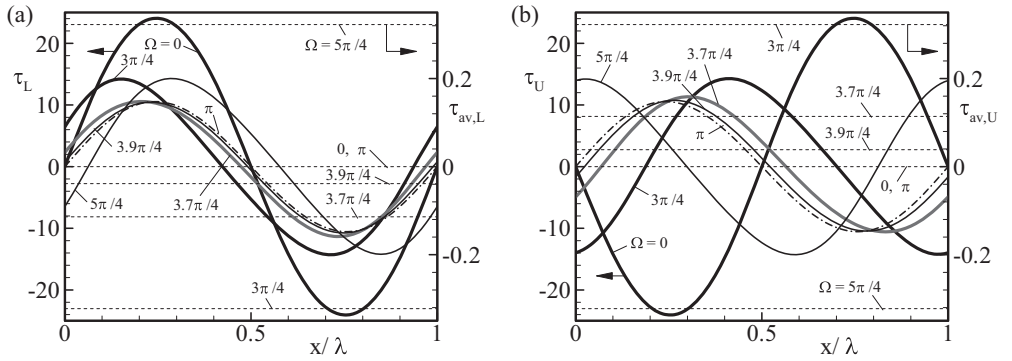

FIG. 3. Distributions of the local shear stress (solid and dashed lines) and its average taken over one heating wavelength (dotted lines) acting on the fluid at the lower (a) and upper (b) walls for conditions corresponding to Fig. 2. The dashed-dotted line corresponds to the local shear stress for $\Omega = \pi$.

$\Omega = 3.7\pi/4$. Part of the fluid volume is permanently trapped inside either the upper or lower sections of the slot and, thus, contributes little to the heat transport. The vertical, highly tilted columns of hotter fluid moving upwards and colder fluid moving downwards can still be recognized. The formation of two roll layers is nearly completed at $\Omega = 3.9\pi/4$ [Fig. 2(d)] with most of the fluid trapped inside the new roll centers. Two distinct roll layers exist at $\Omega = \pi$ [Fig. 2(e)] with half of the fluid permanently trapped in the lower section of the slot and the remaining fluid trapped in the upper section. The upper and lower rolls rotate in the opposite directions resulting in the formation of two layers of heated and cooled fluid, with the zones of heated fluid in the lower layers shifted by half of a wavelength in the horizontal directions with respect to the heated zones in the upper layer. The location of the warmer fluid corresponds to the upward fluid motion in both layers. Further increase of Ω results in reversed changes to what has been described above; the form of these changes can be deduced from the horizontal periodicity conditions. The case of $\Omega = 5\pi/4$ is shown in Fig. 2(f) for illustration purposes.

Figure 3 illustrates distributions of the wall shear acting on the fluid for conditions taken from Fig. 2. These distributions have interesting features depending on how the averages are taken. When $\Omega = 0$, equal and opposite stresses act at the upper and lower walls resulting in zero net stress at each vertical slot section as well as zero mean stress at each wall when averaged over the complete heating wavelength or zero mean stress for both walls when averaged over half of the heating wavelength. This symmetry is lost when Ω increases, resulting in the appearance of a nonzero net stress at each vertical section as well as in a nonzero mean stress at each wall when averaged over one heating period. The latter stress acts in the negative direction at the lower wall and in the positive direction at the upper wall. Distributions of both stresses become identical for $\Omega = \pi$ resulting in a nonzero net stress acting at each vertical slot section and a nonzero mean stress at each wall when averaged over half of the heating wavelength. Since each half gives an opposite direction of the mean shear, their sum gives zero average shear over the full heating wavelength. Further increase of the phase shift until $\Omega = 2\pi$ results in similar variations of shear but with the directions of shear reversed when compared with their directions for $0 < \Omega < \pi$; details of these changes can be deduced from Fig. 3 with the help of the periodicity condition. Results for $\Omega = 5\pi/4$ are shown for illustration purposes.

Variations of the average shear (over one heating period) acting at each wall as a function of Ω are illustrated in Fig. 4(a) for $\mathrm{Ra}_{p,L} = \mathrm{Ra}_{p,U} = 200, 400, 1000$. At the lower wall the mean shear increases slowly from $\tau_{av,L} = 0$ at $\Omega = 0$, reaches a maximum for $\pi/2 < \Omega < \pi$, drops down to zero at $\Omega = \pi$,

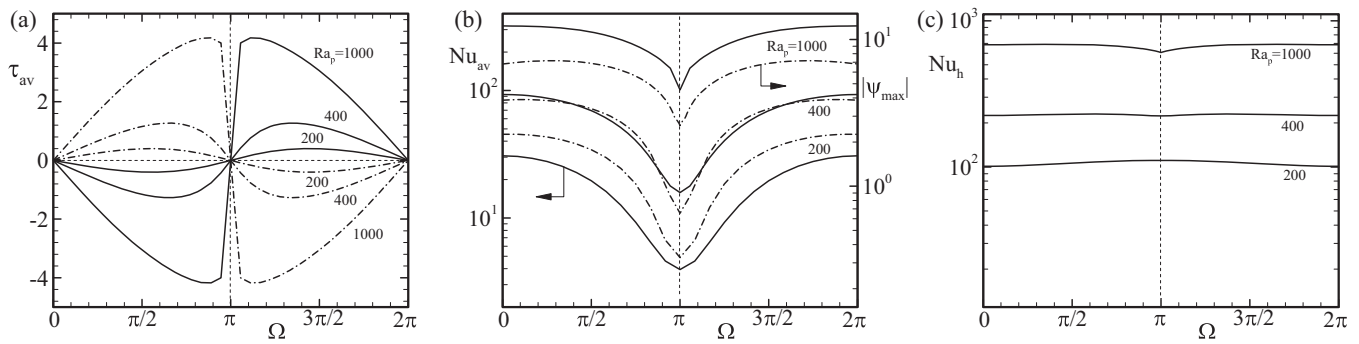

FIG. 4. Variations of the average shear stress acting on the fluid at the lower and the upper walls as functions of the phase shift Ω are displayed in (a) with the solid lines used in the former case and the dash-dotted lines in the latter case. The maximum of the absolute value of the stream function $|\psi_{\max}|$ and the average Nusselt number Nu_{av} as functions of the phase shift Ω are displayed in (b) with the solid lines used in the former case and the dash-dotted lines in the latter. Variations of the horizontal Nusselt number $\mathrm{Nu}_h = \mathrm{Nu}_{h,U} = \mathrm{Nu}_{h,L}$ as a function of the phase shift Ω for $\mathrm{Ra}_{p,L} = \mathrm{Ra}_{p,U} = 200, 400, 1000$ and $\mathrm{Pr} = 0.71$, $\alpha = 1.6$, are shown in (c).

TABLE I. Variations of the intensity of convection as measured by the maximum of the stream function $|\psi_{\max}|$ as a function of the phase shift Ω.

$\mathrm{Ra}_{p,L}(=\mathrm{Ra}_{p,U})$	$\lvert\psi_{\max}(\Omega=0)\rvert$	$\lvert\psi_{\max}(\Omega=\pi)\rvert$	$\lvert\psi_{\max}(\Omega=0)\rvert/\lvert\psi_{\max}(\Omega=\pi)\rvert$
200	2.26	0.33	6.92
400	3.86	0.65	5.90
1000	6.81	2.59	2.68
$\lvert\psi_{\max}(\mathrm{Ra}=400)\rvert/\lvert\psi_{\max}(\mathrm{Ra}=200)\rvert$	1.71	2.01	
$\lvert\psi_{\max}(\mathrm{Ra}=1000)\rvert/\lvert\psi_{\max}(\mathrm{Ra}=400)\rvert$	1.76	3.96	

changes sign and follows a similar pattern for $\pi < \Omega < 2\pi$ dropping again down to zero at $\Omega = 2\pi$. The distribution of $\tau_{av,L}$ is antisymmetric with respect to $\Omega = \pi$ as dictated by the periodicity condition. The mean shear at the upper wall has exactly the same magnitude and distribution but the opposite direction. Increase of the heating intensity results in much larger magnitudes of $\tau_{av,L}$ and $\tau_{av,U}$ with the maxima moving closer to $\Omega = \pi$ and the appearance of very large gradients of $d(\tau_{av,L})/d\Omega$ and $d(\tau_{av,U})/d\Omega$ in the vicinity of $\Omega = \pi$. Use of spatially variable heating implies heat flow along the walls. Figure 4(c) illustrates distributions of the horizontal Nusselt numbers $\mathrm{Nu}_{h,U}$ and $\mathrm{Nu}_{h,L}$, which are the same along both walls and exhibit minor variations as functions of Ω.

Existence of a nonzero mean shear leads to the generation of a net force acting on each wall. This is an interesting effect as convection within one cell is able to generate a global effect reaching beyond this cell. This force, summed over several convection cells, could add up to a sizable magnitude and could lead to a change in the relative positions of both walls assuming that the walls are allowed to move and assuming that the heating patterns are fixed with respect to each wall during such movement. We shall refer to this effect as thermally induced drift. The directions of the forces acting on the walls are such that the phase shift $\Omega = \pi$ corresponds to an unstable equilibrium and the phase shifts $\Omega = 0, 2\pi$ correspond to stable equilibria. Assuming that drift is allowed, the system will eventually end up in a position where the hot spots are located above each other, i.e., $\Omega = 0, 2\pi$, with the final flow topology illustrated in Fig. 2(a). Further interesting system properties can be identified by allowing stretching of the boundaries, e.g., boundaries formed by stretchable membranes. For example, when $\Omega = \pi$, membranes on both walls are pulled in the same direction within each half heating wavelength (τ_U and τ_L act in the same direction) while for $\Omega = 0$ they are pulled in the opposite directions (τ_U and τ_L act in the opposite directions) (see Fig. 3).

Changes in the flow topology and the temperature field discussed above suggest significant variations of the intensity of convection as well as the net heat flow between the walls as functions of Ω. The former can be measured using the absolute value of the maximum of the stream function $|\psi_{\max}|$. Its distributions presented in Fig. 4(b) demonstrate that the intensity is always largest for $\Omega = 0$ and smallest for $\Omega = \pi$. Detailed comparisons presented in Table I demonstrate a rapid increase in the intensity of convection as Rayleigh numbers increase, as well as its progressive equilibration between $\Omega = 0$ and $\Omega = \pi$. The resulting changes of the heat flow are also illustrated in Fig. 4(b) using the average Nusselt number Nu_{av}. Detailed comparisons presented in Table II demonstrate that an increase of the Rayleigh numbers causes a rapid increase of Nu_{av} as well as its equilibration between $\Omega = 0$ and $\Omega = \pi$ which underline the close connection between the net heat flow and the intensity of convection. If the wall drift were allowed, the system would eventually end up in a position corresponding to $\Omega = 0$ which produces the maximum net heat flow.

The above discussion is based on the results for a single heating wavelength, i.e., $\alpha = 1.6$. The effect of changing the heating wavelength on the average shear can be deduced from data presented in Fig. 5 for $\mathrm{Ra}_{p,L} = \mathrm{Ra}_{p,U} = 200$. The average shear acting at the lower wall [Fig. 5(a)] has two extrema at $\alpha \approx 1.6$, one for $\Omega = \Omega_{\max,\tau} \approx \pi/2$ and another for $\Omega_{\max,\tau} \approx 3\pi/2$. These extrema have the same magnitude but opposite signs which account for the change in the direction of rotation of the convective roll. The magnitude of $\tau_{av,L}$ decreases to zero for both $\alpha \to 0$ and $\alpha \to \infty$; its variations are antisymmetric with respect to $\Omega = \pi$ for all α's and values are negative when $0 < \Omega < \pi$ and positive when $\pi < \Omega < 2\pi$. The average shear acting at the upper wall has the same distribution but the opposite direction [see Fig. 5(b)]. Variations of the maximum of the absolute value of the stream function displayed in Fig. 6(a) demonstrate that $|\psi_{\max}|$ has two global maxima occurring at $\alpha \approx 0.9$, one corresponding to $\Omega_{\max,\psi} \approx \pi/4$ and one for $\Omega_{\max,\psi} \approx 7\pi/4$. An increase or decrease of α away from $\alpha \approx 0.9$ moves the local maxima either to $\Omega_{\max,\psi} = 0$ or to $\Omega_{\max,\psi} = 2\pi$. The minimum always occurs for $\Omega_{\max,\psi} = \pi$ regardless of α and the distribution is always symmetric with respect to $\Omega = \pi$. The above discussion shows that the qualitative features of

TABLE II. Variations of the average Nusselt number Nu_{av} as a function of the phase shift Ω.

$\mathrm{Ra}_{p,L}(=\mathrm{Ra}_{p,U})$	$\mathrm{Nu}_{av}(\Omega=0)$	$\mathrm{Nu}_{av}(\Omega=\pi)$	$\mathrm{Nu}_{av}(\Omega=0)/\mathrm{Nu}_{av}(\Omega=\pi)$
200	30.74	3.93	7.81
400	93.71	15.81	5.88
1000	320.68	118.41	2.71
$\mathrm{Nu}_{av}(\mathrm{Ra}_{p,L}=400)/\mathrm{Nu}_{av}(\mathrm{Ra}_{p,L}=200)$	3.05	4.02	
$\mathrm{Nu}_{av}(\mathrm{Ra}_{p,L}=1000)/\mathrm{Nu}_{av}(\mathrm{Ra}_{p,L}=400)$	3.42	7.49	

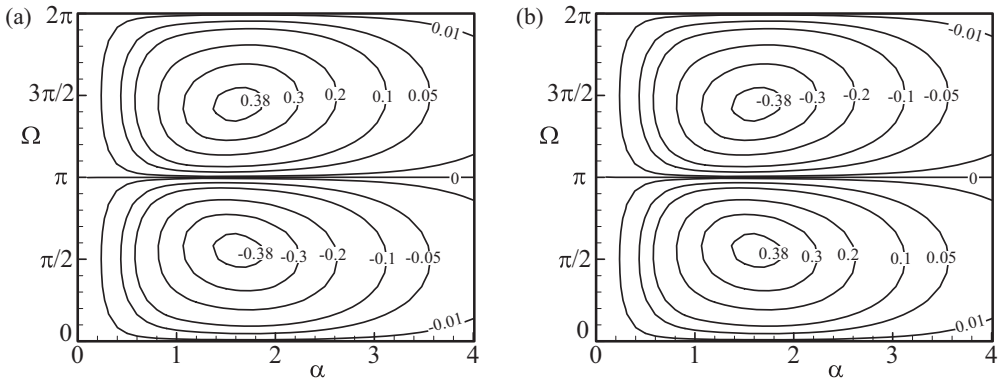

FIG. 5. Variations of the average wall shear stress acting on the fluid at the lower (a) and upper (b) walls as functions of the heating wave number α and the phase shift Ω for $\mathrm{Ra}_{p,L} = \mathrm{Ra}_{p,U} = 200$, $\mathrm{Pr} = 0.71$.

distributions of τ_{av} and $|\psi_{\max}|$ are different as the global maxima do not overlap. Figure 6(b) displays distribution of Nu_{av}. The global maxima occur for $\alpha \approx 1.2$ and correspond to $\Omega_{\max,\mathrm{Nu}} = 0,2\pi$. The heat transfer decreases to zero for both $\alpha \to 0$ and $\alpha \to \infty$.The lowest heat flow corresponds to $\Omega = \pi$ with distribution of Nu_{av} being symmetric with respect to $\Omega = \pi$. Again, the distribution of Nu_{av} does not correlate well with the distributions of $\tau_{av,L}$ and $|\psi_{\max}|$. Variations of $\mathrm{Nu}_h (= \mathrm{Nu}_{h,U} = \mathrm{Nu}_{h,L})$ illustrated in Fig. 6(c) demonstrate that the horizontal heat flow does not change appreciably as a function of Ω for all α's except $\alpha < 1$. The largest Nu_h always corresponds to $\Omega_{\max,\mathrm{Nu}_h} = \pi$.

The effect of increasing the heating intensity can be deduced by comparing distributions of $\tau_{av,L}$, $|\psi_{\max}|$, and Nu_{av} for $\mathrm{Ra}_{p,L} = \mathrm{Ra}_{p,U} = 200$ displayed in Figs. 5 and 6 with distributions for $\mathrm{Ra}_{p,L} = \mathrm{Ra}_{p,U} = 400$ displayed in Fig. 7 and with distributions for $\mathrm{Ra}_{p,L} = \mathrm{Ra}_{p,U} = 1000$ displayed in Fig. 8. The maximum average wall shear moves towards larger α's as Ra increases with the corresponding $\Omega_{\max,\tau}$ coming closer to $\Omega_{\max,\tau} = \pi$ [compare Figs. 5(a), 7(a), and 8(a)]. At the same time, the maxima of $|\psi_{\max}|$ move towards smaller α's and also come closer to $\Omega_{\max,\psi} = \pi$ [compare Figs. 6(a), 7(b), and 8(b)]. The maxima of Nu_{av} likewise move towards smaller α's but always correspond to $\Omega_{\max,\mathrm{Nu}} = 0,2\pi$ [compare Figs. 6(b), 7(c), and 8(c)]. Conditions resulting in the largest average shear, the most intense convection, and the largest heat flow do not correlate well with each other in the (α, Ω) plane for all Ra's considered.

Figure 9 illustrates the properties of the system for different heating intensities applied at each wall. The lower wall has a constant heating corresponding to (i) $\mathrm{Ra}_{p,L} = 500$ and (ii) $\mathrm{Ra}_{p,L} = 1000$ while heating of the upper wall gradually increases. The average wall shear stress is zero at each wall when only one wall is heated [see Figs. 9(a) and 9(c)]. The magnitude of τ_{av} increases with an increase of $\mathrm{Ra}_{p,U}$, the increase is the same at both walls, and τ_{av} reaches the maximum when $\mathrm{Ra}_{p,U}$ reaches the largest value considered. The phase shift, which produces the highest τ_{av}, changes from $\Omega \approx \pi/2$ for small $\mathrm{Ra}_{p,U}$ to $\Omega \approx 2\pi/3$ at $\mathrm{Ra}_{p,U} = 1000$ when $\mathrm{Ra}_{p,L} = 500$, and to $\Omega \approx 9\pi/10$ when $\mathrm{Ra}_{p,L} = 1000$. The phase shift which produces the maximum τ_{av} for $\pi < \Omega < 2\pi$ can be determined from the antisymmetry conditions. The evolution of $|\psi_{\max}|$ as a function of $\mathrm{Ra}_{p,U}$ is illustrated in Figs. 9(b) and 9(d). $|\psi_{\max}|$ for heating applied at one wall provides the reference point. When $\mathrm{Ra}_{p,L} = 1000$, an increase of $\mathrm{Ra}_{p,U}$ results in a decrease of the convection intensity for a range of Ω centered around $\Omega \approx \pi$ and an increase everywhere else with the largest increase taking place for $\Omega = 5\pi/18$. When $\mathrm{Ra}_{p,L} = 500$, an increase of $\mathrm{Ra}_{p,U}$ results in an increase of convection intensity for all Ω with the largest one taking place when $\Omega = 2\pi/9$. Detailed data are given in Table III.The same figures illustrate changes of Nu_{av} as a function of $\mathrm{Ra}_{p,U}$ with the reference point given by Nu_{av} for one wall being

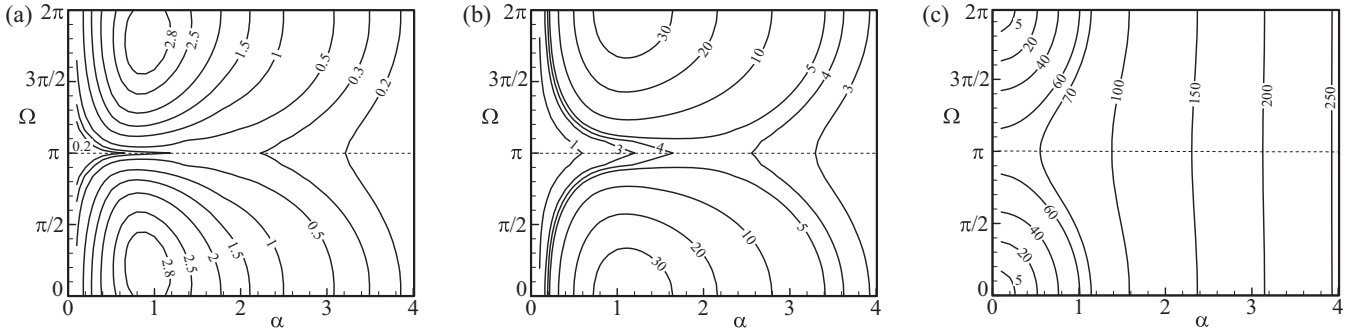

FIG. 6. Variations of the maximum of the absolute value of the stream function $|\psi_{\max}|$ (a), the average Nusselt number Nu_{av} (b), and the horizontal Nusselt number $\mathrm{Nu}_h = \mathrm{Nu}_{h,U} = \mathrm{Nu}_{h,L}$ (c) as functions of the heating wave number α and the phase shift Ω for $\mathrm{Ra}_{p,L} = \mathrm{Ra}_{p,U} = 200$, $\mathrm{Pr} = 0.71$.

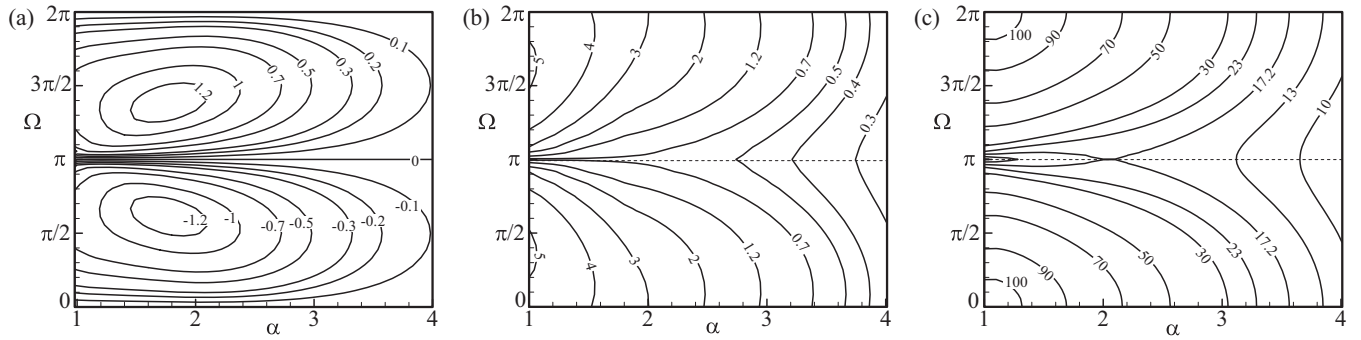

FIG. 7. Variations of the average wall shear stress acting on the fluid at the lower wall (a), the maximum of the absolute value of the stream function $|\psi_{\max}|$ (b), and the average Nusselt number Nu_{av} (c) as functions of the heating wave number α and the phase shift Ω for $\mathrm{Ra}_{p,L} = \mathrm{Ra}_{p,U} = 400$, $\mathrm{Pr} = 0.71$.

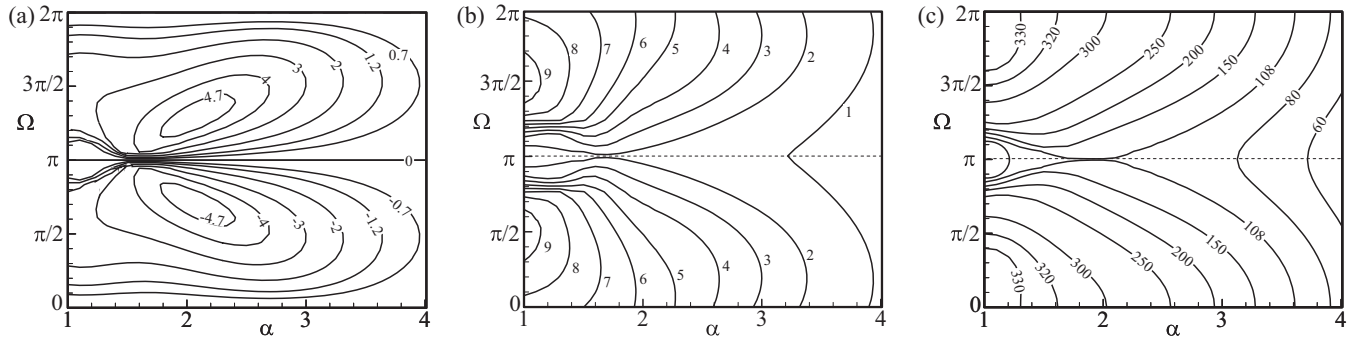

FIG. 8. Variations of the average wall shear stress acting on the fluid at the lower wall (a), the average Nusselt number Nu_{av} (b), and the maximum of absolute value of the stream function $|\psi_{\max}|$ (c) as functions of the heating wave number α and the phase shift Ω for $\mathrm{Ra}_{p,L} = \mathrm{Ra}_{p,U} = 1000$, $\mathrm{Pr} = 0.71$.

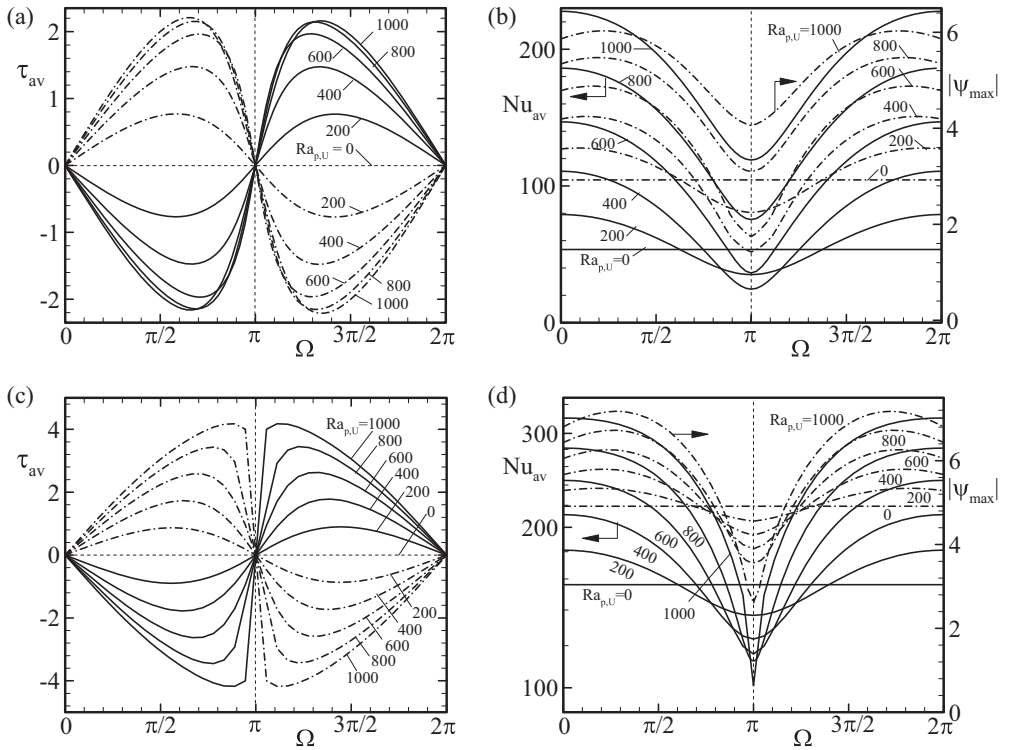

FIG. 9. Variations of the average shear stress acting on the fluid at (a) the lower (solid lines) and the upper (dash-dotted lines) walls; (b) the average Nusselt number Nu_{av} (solid lines) and the maximum of the stream function $|\psi_{\max}|$ (dash-dotted lines) as functions of the phase shift Ω for $\mathrm{Ra}_{p,L} = 1000$, $\mathrm{Pr} = 0.71$, $\alpha = 1.6$ and $\mathrm{Ra}_{p,U} = 0$, 200, 400, 600, 800, 1000. (c), (d) display the same quantities but for $\mathrm{Ra}_{p,L} = 500$.

TABLE III. Variations of the intensity of convection as measured by the maximum of the stream functions $|\psi_{\max}|$ and the average Nusselt number Nu_{av} as functions of the phase shift Ω and the upper periodic Rayleigh number $\mathrm{Ra}_{p,U}$ for the fixed lower periodic number $\mathrm{Ra}_{p,L}$.

$\mathrm{Ra}_{p,L}$	$\mathrm{Ra}_{p,U}$	$\tau_{av}(\Omega = 9\pi/10)$	$\lvert\psi_{\max}(\Omega = \pi)\rvert$	$\lvert\psi_{\max}(\Omega = 5\pi/18)\rvert$	$\mathrm{Nu}_{av}(\Omega = \pi)$	$\mathrm{Nu}_{av}(\Omega = 0)$
1000	0	0	4.91	4.91	156.11	156.11
	1000	4.17	2.59	7.18	100.99	320.68
	% change	N/A	−42.7	+46.1	−35.3	+105.7
$\mathrm{Ra}_{p,L}$	$\mathrm{Ra}_{p,U}$	$\tau_{av}(\Omega = 2\pi/3)$	$\lvert\psi_{\max}(\Omega = \pi)\rvert$	$\lvert\psi_{\max}(\Omega = 2\pi/9)\rvert$	$\mathrm{Nu}_{av}(\Omega = \pi)$	$\mathrm{Nu}_{av}(\Omega = 0)$
500	0	0	2.92	2.92	53.51	53.51
	1000	2.18	4.06	6.03	118.95	227.73
	% change	N/A	+39.0	+106.5	+122.3	+325.6

heated. When $\mathrm{Ra}_{p,L} = 1000$, the heat flow decreases for a range of Ω centered around $\Omega \approx \pi$ and increases everywhere else with the largest increase taking place for $\Omega = 0$ regardless of the value of $\mathrm{Ra}_{p,L}$. When $\mathrm{Ra}_{p,L} = 500$, an increase of $\mathrm{Ra}_{p,U}$ results in an increase of Nu_{av} for all Ω with the largest one taking place when $\Omega = 0$. Detailed data are presented

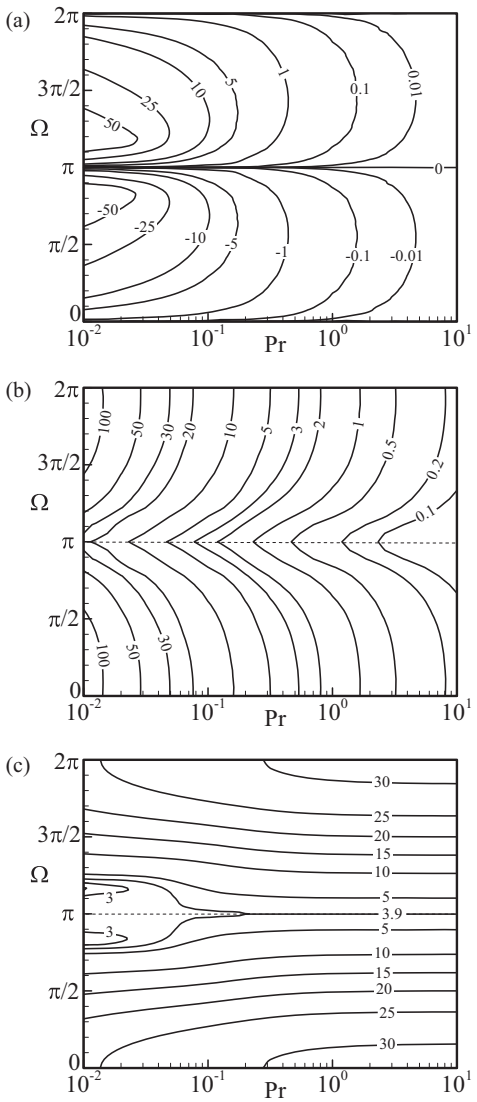

FIG. 10. Variations of the average wall shear stress acting on the fluid at the lower wall (a), the maximum of the absolute value of the stream function $|\psi_{\max}|$ (b), and the average Nusselt number Nu_{av} (c) as functions of the Prandtl number Pr and the phase shift Ω for the heating wave number $\alpha = 1.6$ and $\mathrm{Ra}_{p,L} = \mathrm{Ra}_{p,U} = 200$.

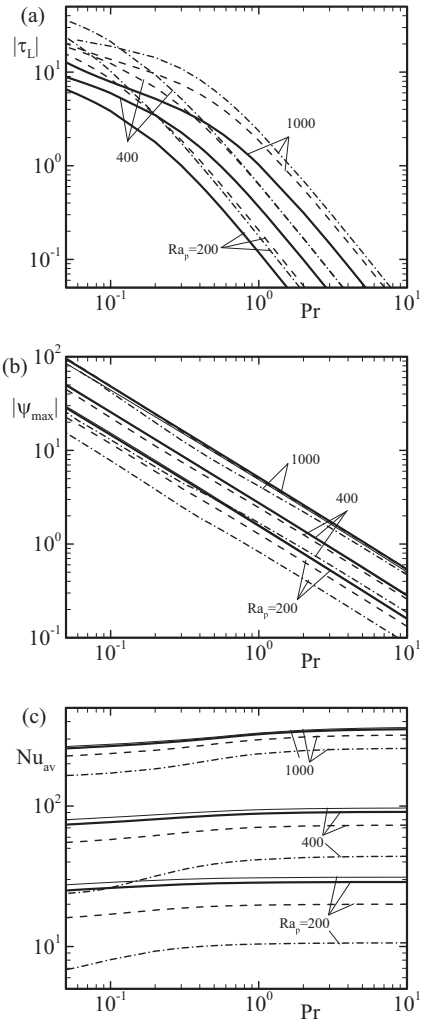

FIG. 11. Variations of the average wall shear stress acting on the fluid at the lower wall (a), the maximum of the absolute value of the stream function $|\psi_{\max}|$ (b), and the average Nusselt number Nu_{av} (c) as functions of the Prandtl number Pr for the phase shift $\Omega = 0$, $\pi/4$, $\pi/2$, $3\pi/4$ for the heating wave number $\alpha = 1.6$ and $\mathrm{Ra}_{p,L} = \mathrm{Ra}_{p,U} = 200$, 400, 1000. Solid, dashed, and dash-dotted lines are for $\Omega = \pi/4$, $\pi/2$, $3\pi/4$, respectively. In (a), $\tau_L = 0$ for $\Omega = 0$ (not shown); (b), (c) thin solid line represents $\Omega = 0$.

in Table III. These results demonstrate that changes of all quantities become more extreme with an increase of $\mathrm{Ra}_{p,L}$.

The results discussed above deal with fluids with $\mathrm{Pr} = 0.71$. The effect of changes of the fluid thermophysical properties can be deduced from data presented in Figs. 10 and 11. The basic features of the convection remain the same at any value of the Prandtl number. The magnitude of the average stress increases as Pr decreases as documented in Fig. 10(a). This is the result of an increase of the intensity of convection with reduction of Pr as documented in Fig. 10(b). The net heat transfer decreases with a decrease of Pr as changes in the temperature field induced by convection are less important when compared with the conductive component of the temperature field, as documented in Fig. 10(c). All these processes are approximately similar in the range of Rayleigh numbers considered in this study, with the more extreme values found for higher Ra's, as documented in Fig. 11.

IV. SUMMARY

Natural convection in a horizontal slot subject to periodic heating applied at the upper and lower walls has been analyzed. The upper heating has been shifted with respect to the lower heating by a phase shift Ω. The fluid properties have been represented using the Boussinesq approximation. The system dynamics are parametrized by the amplitudes of the upper and lower heatings expressed in terms of the lower and upper Rayleigh numbers, i.e., $\mathrm{Ra}_{p,L}$ and $\mathrm{Ra}_{p,U}$, the heating wavelength $\lambda = 2\pi/\alpha$, and the phase shift Ω. A significant change in the convection pattern has been observed as Ω varies from 0 to 2π. This pattern generally consists of one layer of pairs of counter-rotating rolls but morphs into two layers for $\Omega \approx \pi$. Changes of Ω result in significant variations in the intensity of convection, with the weakest convection corresponding to $\Omega = \pi$ and the strongest convection taking place for Ω closest to 0 and 2π. This convection creates a wall shear stress with a nonzero mean for all phase shifts except $\Omega = 0$, π, 2π. The mean shear, when summed over several heating wavelengths, may lead to the generation of a sizable force which could lead to a drift in the relative position of both walls. This effect, which is referred to as the thermally induced drift, demonstrates the ability of a single convection cell to create a global force. Changes of Ω also lead to changes in the net heat flow between the walls, with the smallest heat flow occurring for $\Omega = \pi$ and the largest for $\Omega = 0$, 2π. The properties of the convective system remain qualitatively similar for all values of the Prandtl number, with the mean shear and the convection intensity increasing and the net heat flow decreasing with reduction of Pr.

ACKNOWLEDGMENT

This work has been carried out with the support of NSERC of Canada.

[1] H. Bénard, Rev. Gen. Sci. Pure Appl. **11**, 1261 (1900).
[2] J. W. S. Rayleigh, Philos. Mag. **32**, 529 (1916).
[3] E. Bodenschatz, W. Pesch, and G. Ahlers, Ann. Rev. Fluid Mech. **32**, 709 (2000).
[4] G. Ahlers, S. Grossmann, and D. Lohse, Rev. Mod. Phys. **81**, 503 (2009).
[5] D. Lohse and K. Q. Xia, Annu. Rev. Fluid Mech. **42**, 335 (2010).
[6] F. Chilla and J. Schumacher, Eur. Phys. J. E **35**, 58 (2012).
[7] G. Freund, W. Pesch, and W. Zimmermann, J. Fluid Mech. **673**, 318 (2011).
[8] T. Maxworthy, Annu. Rev. Fluid. Mech. **29**, 327 (1997).
[9] G. O. Hughes and R. W. Griffiths, Annu. Rev. Fluid Mech. **40**, 185 (2008).
[10] J. H. Siggers, R. R. Kerswell, and N. J. Balmforth, J. Fluid Mech. **517**, 55 (2004).
[11] K. B. Winters and W. R. Young, J. Fluid Mech. **629**, 221 (2009).
[12] M. Z. Hossain and J. M. Floryan, Phys. Rev. E **90**, 023015 (2014).
[13] M. Z. Hossain and J. M. Floryan, ASME J. Heat Transfer **135**, 022503 (2013).
[14] A. Lenardic, L. Moresi, A. M. Jellinek, and M. Manga, Earth Planet. Sci. Lett. **234**, 317 (2005).
[15] S. Marcq and J. Weiss, Cryosphere **6**, 143 (2012).
[16] P. Ripesi, L. Biferale, M. Sbragaglia, and A. Wirth, J. Fluid Mech. **742**, 636 (2014).
[17] A. M. Rizwam, L. Y. C. Dennis, and C. Liu, J. Environ. Sci. **20**, 120 (2008).
[18] M. A. Finney, J. D. Cohen, S. S. McAllister, and W. M. Jolly, Int. J. Wildland Fire **22**, 25 (2013).
[19] M. Z. Hossain and J. M. Floryan, J. Fluid Mech. **733**, 33 (2013).
[20] J. P. Rothstein, Annu. Rev. Fluid Mech. **42**, 89 (2010).
[21] J. M. Floryan, Bull. Am. Phys. Soc. **57**(1), X50.00015 (2012).
[22] M. Z. Hossain, D. Floryan, and J. M. Floryan, J. Fluid Mech. **713**, 398 (2012).
[23] D. Floryan and J. M. Floryan, J. Fluid Mech. **765**, 353 (2015).
[24] M. Z. Hossain and J. M. Floryan, J. Fluid Mech. **768**, 51 (2015).
[25] C. Canuto, M. Y. Hussaini, A. Quarteroni, and T. A. Zang, *Spectral Methods: Fundamentals in Single Domains* (Springer-Verlag, Berlin, Heidelberg, 2006).